Asian Journal of Physics
Vol. 33, No 12 (2024) 765-774
Available on: www.asianjournalofphysics.com

ap

A 2-D subset of Nano Fraction

C A Sciammarella[1], L Lamberti[2], E Sciammarella[3], and F M Sciammarella[4]

[1]*Department of Mechanical, Materials and Aerospace Engineering,*

Illinois Institute of Technology, 10 32nd SW St, Chicago, IL 60616, USA

[2]*Dipartimento di Meccanica, Matematica e Management, Politecnico di Bari, Viale Orabona 4, Bari, 70125 Italy*

[3]*NanoFraction Inc., Chicago, IL 60611 USA*

[4]*Tekna Solutions, 1600 S. Praire Avenue, Chicago, IL 60616, USA*

Dedicated to Prof (Dr) Daniel Malacara-Hernández

This paper presents a subset of an optical system designed to retrieve spatial information with extremely high spatial and temporal resolutions. The system, referred to as Nano Fraction (NF), utilizes lasers with wavelengths ranging from 400 to 700 nm to capture images of objects in the nanometer range. NF encompasses techniques such as Holographic Moiré (MOH), Evanescent Illumination, Broadened Brillouin Scattering (BBS), and Super-resolution (SR). The article focuses on developing a model for Brillouin scattering in two-dimensional lattices to address photon-phonon interaction issues within the general context of NF. Given the complexity of the subject, a 2-D version of the methodology is presented. The authors have extended this approach to 3-D. This extension will be the subject of future publications.

doi: 10.54955.AJP.33.12.2024.765-774

Keywords: Light scattering; Brillouin Scattering (induced and broadened), Crystalline structures, Photon-phonon interactions, Light emission of materials, Wavelength and velocity of generated waves, 2-D measurements of prismatic crystals.

1 Introduction

The Nano Fraction (NF) system [1] is a state-of-the-art optical system for nano-scale measurements based on moiré-holography, evanescent illumination, Brillouin scattering, and super resolution. NF uses lasers with wavelengths between 400 and 700 nm to capture images of objects in the nanometer range, retrieving spatial information with very high spatial and temporal resolutions.

This paper focuses on developing a model for Brillouin scattering [2,3] in two-dimensional lattices to address photon-phonon interaction issues that relate to the geometry and properties of the lattices. This model also introduces a variable: the wavelength of the scattered light λ_{sct} emitted by the medium under analysis. The notion of *Brillouin Scattering* originated in the work associated with the measurement of the speed of sound using light scattering. Subsequently, it was discovered that Brillouin scattering could be observed with laser illumination, and the nomenclature *Induced Brillouin* Scattering was introduced. The original work of Brillouin was based on the analysis of crystals. Garmire [4] generalized the validity of Brillouin scattering to any media and state of matter resorting to the introduction of continuum Physics principles: she called this extension Broad Brillouin Scattering [BBS].

Corresponding author
e mail:luciano.lamberti@poliba.it (L Lamberti)

2 Model for Brillouin scattering

Different ways can be utilized to derive the relationships that are a consequence of the Brillouin scattering for 2-D lattices. One can go the way of solutions of the Maxwell equations: this approach was followed by Russian authors resulting in solutions carrying the names of the authors. A detailed description of this approach and work done on these topics is given in Lakhtakia *et al* [5]. The method to achieve this objective is to outline the setup used for the measurements that support the results presented in this paper. Rucker [6] suggests that human sensory perception equips us with information within a four-dimensional framework: three spatial and one temporal dimension. When we attempt to explain phenomena observed through experimentation, it is essential to recognize that our understanding of reality can vary with the dimensions included in the chosen model. When we link the multidimensional world with the four-dimensional Newtonian mechanics, using a scheme similar to the one shown in Fig 1, it is necessary to acknowledge that we are focusing on specific optical observations. This paper will adopt the approach originally introduced by Chiao in his Ph D dissertation [7]. We begin with a graphical drawing inspired by Feynman diagrams, which visually represents the mathematical equations describing the behavior and interaction of subatomic particles.

3 Photon-Phonon interaction graphical representation

Figure 1, inspired by Feynman diagrams, visually represents the mathematical equations describing the behavior and interaction of subatomic particles. The circles represent the particle nature of photons and photons. The sinusoids represent the particle's dual nature as waves. The diameters of the circles represent energy. A larger diameter represents higher energy. The colors represent the wavelengths. The brown color is selected to represent phonons. The significance of the diagram lies in the trajectory directions of photons and phonons, as illustrated by the small triangle in Fig 1. This triangle is a bridge that connects Quantum Mechanics and Newtonian Mechanics. $\mathbf{K}_L$ represents the vector momentum of the illuminating light. $\mathbf{K}_{sct}$ is the momentum vector of the scattered light, while $\mathbf{K}_{ac}$ denotes the vector momentum of the acoustic wave. The respective angular frequencies ω correspond to the energies of the wavefronts. The other quantity involved is θ_{icr} and comes from Feynman's diagram spatial orientation, the relationship is valid if the angle between the two vectors is θ_{icr}. Let us introduce the quantities involved in the preservation of energy and momentum.

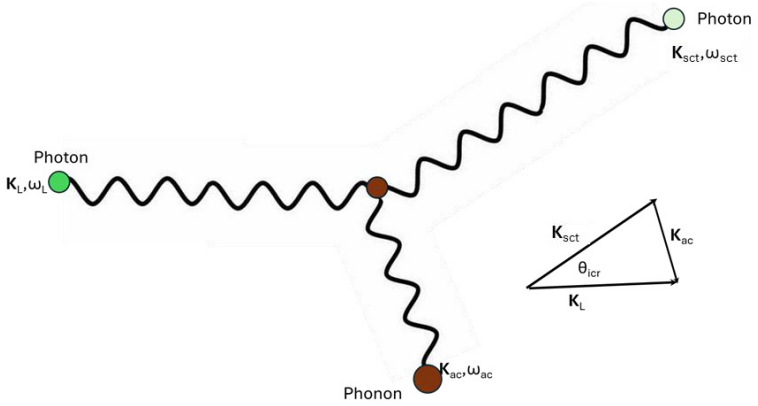

Fig 1. Photon-phonon impact diagram.

Table 1 The derivations developed in the following sections utilize the nomenclature conventions used in Fig 1 and the corresponding definitions given in Table 1. The conservation of energy is expressed as:

$$\omega_L = \omega_{sct} + \omega_{ac} \tag{1}$$

From Eq (1), it follows:

$$\omega_{sct} = \omega_L - \omega_{ac} \tag{2}$$

Table 1. Definition of angular frequencies involved in the photon-photon interaction.

ω_L	$2\pi/\lambda_L$
ω_{sct}	$2\pi/\lambda_{sct}$
ω_{ac}	$2\pi/\Lambda_{ac}$

In scattering processes, when the resulting scattered wave of angular frequency ω_{sct} experiences a down shift in angular frequency, it is referred to as a Stokes wave. Conversely, if the frequency increases during scattering, the wave is known as an anti-Stokes wave. During the interaction between phonons and photons, momentum conservation applies. Figure 2 is an enlarged version of the small triangle in Fig 1. This indicates that the vector equation, as illustrated in the diagram of Fig 2, must be fulfilled to ensure the conservation of momentum.

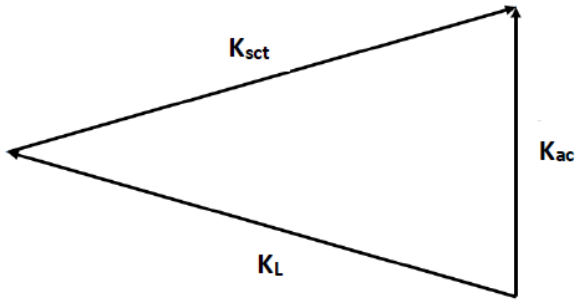

Fig 2. Graphical representation of the vectorial equations describing the preservation of momentum.

Figure 2 utilizes the same notations of Table 1 including subscripts *ac*, *L* and *sct*. The corresponding vectorial equation is:

$$\boldsymbol{K}_{ac} = \boldsymbol{K}_L + \boldsymbol{K}_{sct} \tag{3}$$

Equation (3) is the relationship connecting the corresponding momenta. Now, we will consider the possibilities of relative orientations of the corresponding wavefronts. The largest modulus of the acoustic vector takes place when the scattered light is anti-Stokes. In the anti-Stokes condition, the magnitude of the vectors of Eq (3) obey the relationship,

$$|\boldsymbol{K}_{sct}| = |\boldsymbol{K}_L| + |\boldsymbol{K}_{ac}| \tag{4}$$

In Eq (4), the brackets indicate the magnitudes of the corresponding vectors. The magnitudes of the momentum vectors are determined by dividing the angular velocity by the wave velocity in the respective medium. By applying this relationship to Eq (4), one can derive the following result:

$$\frac{\omega_{ac}}{v_{ac}} = \frac{\omega_L}{v_L} = \frac{\omega_{sct}}{v_{sct}} \tag{5}$$

The previous derivations rely and focus on fundamental principles. In the upcoming analysis, it will be essential to incorporate details about how these principles are applied to a specific setup, including the relevant geometry and operational modes. The classical system designed for making super-resolution measurements using evanescent wavefronts consists of a prism that generates the critical angle of illumination, θ_{icri}. The system being utilized is a variant that incorporates a spherical ball lens into the optical circuit [8].

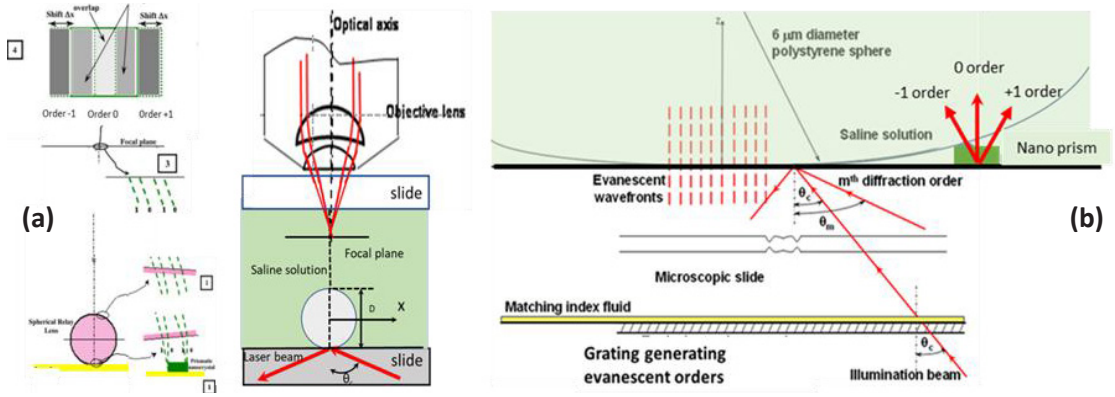

Fig 3. (a) Schematic representation of an optical circuit leading to the formation of an image recorded by a microscope; (b) contact region between the prismatic crystal and the supporting macroscopic slide showing the presence of the grating that generates the diffraction orders.

Figures 3(a) and 3(b) are reproduction of images that illustrate the observations of NaCl nanocrystals recorded by the microscope [8-10]. The ball lens directs the wavefronts generated by the prismatic crystal to its focal plane. The microscope is focused on this focal plane, producing an image of the wavefronts that can be used to determine the geometric configuration of the nanocrystal. With this information, we can now relate the scheme in Fig 1 connecting Newtonian mechanics with the concepts of quantum optics. The first important conclusion is that during transmission, the wavefronts encoding the information pass through the nanocrystal. In Eq (5), v_{ac} represents the ultrasound velocity in the observed NaCl nanocrystal, where the interaction between phonons and photons occurs, v_L is the velocity of the pumping laser light entering the crystal through the contact region. Additionally, v_{sct} refers to the velocity of the scattered light in the crystalline medium NaCl. From Eq (5) through simplifications, it can be obtained:

$$\omega_{ac} = 2\omega_L\left(\frac{v_{ac}}{v_L}\right) \tag{6}$$

Equation (6) approximates Eq (5), considering that the ratio v_{sct}/v_L is of the order of magnitude of 10^{-5}. The graphical consequence of this approximation is illustrated in Fig 4. Using the simplification, $\mathbf{K}_L \approx \mathbf{K}_{sct}$, the triangle of Fig 2 becomes the isosceles triangle of Fig 4.

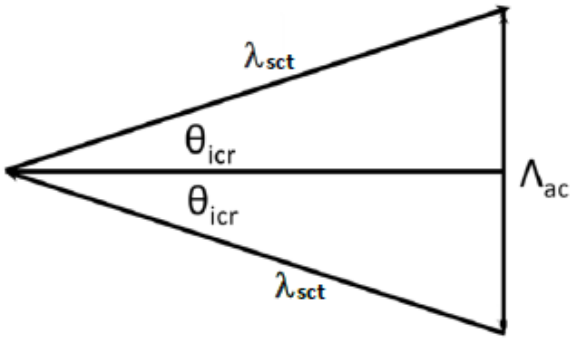

Fig 4. Simplified vectorial equation representing the preservation of the momentum.

The momentums are proportional to the wavelengths of the corresponding wavefronts. Therefore, the values of the momentum vectors can be replaced by their respective wavelengths. In Fig 4, λ_{sct} represents the wavelength of the scattered wavefront inside the crystal, Λ_{ac} represents the wavelength of the acoustic

wave in the medium surrounding the observed object. Then, from the graph of Fig 4, after trigonometric transformations, one can write,

$$2\Lambda_{ac}\ \sin\theta_{icri} = \lambda_{sct} \tag{7}$$

Equation (7) then yields:

$$\sin\theta_{icri} = \lambda_{sct}/(2\Lambda_{ac}) \tag{8}$$

The above Eq (8) was derived by the authors in [8]. This equation applies to diffraction at the Bragg angle. In [8], it was shown that for the standing wave in a crystal one obtains,

$$\sin\theta_{icri} = \lambda_{sct}/\Lambda_{ac} \tag{9}$$

4 Relationship of the BBS with Raman scattering

Raman scattering is another type of light scattering that, like Brillouin scattering (BBS), relies on a model describing the interactions between phonons and photons. In one of its various formulations, it arrives at an equation that is identical to Eq (9),

$$\sin\theta_{icri} = \lambda_{sct}/\Lambda_{ac} \tag{10}$$

Equality is only formal because the same equation represents different phenomena. To explain the relationship between the two scattering forms, a plot of the power vs. frequency is shown in Fig 5.

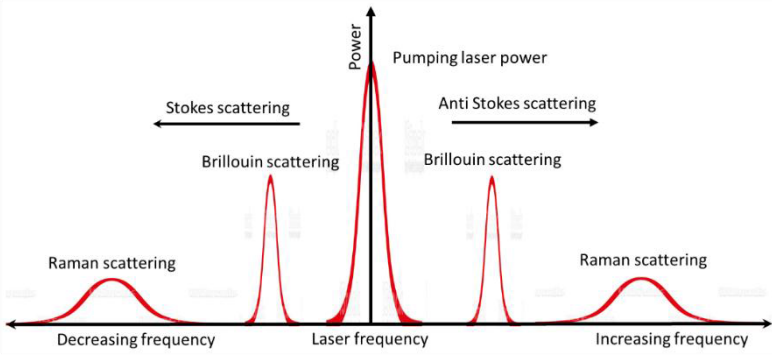

Fig 5. Comparison between frequency shifts and power of the Brillouin/Raman scattering phenomena and power/frequency of a pumping laser.

The Brillouin scattering of Fig 5 holds true only for prisms of a specific length $L_o < L_{crit}$. At the length L_{crit}, the scattered light wavelength does not change further with respect to the laser light wavelength. Figure 5 illustrates that both power and frequency shifts behave differently for Brillouin scattering (BBS) and Raman scattering. The relative frequencies can be either higher or lower than that of the laser depending on whether the scattering is anti-Stokes or Stokes. The designation of Stokes or anti-Stokes depends on whether the light waves are in the same direction as the sound waves (Stokes) or have opposite directions (anti-Stokes). In our application, we are particularly interested in the higher frequencies.

For comparison, the frequencies of Brillouin scattering are given by $f = \omega/2\pi$ typically on the order of magnitude of 10^9 Hz, while for Raman scattering the order of magnitude of frequencies is 10^{13} Hz. This indicates that the fundamental processes underlying each phenomenon differ based on molecular structure. Due to the photoelastic effect, BBS creates pseudo-crystalline structures that depend on the deformation of the observed medium where light propagates. Raman scattering deals with the actual molecular structure of the medium through which the acoustic waves propagate. The geometry of the observed monomers and the connection with the Brillouin scattering are shown in Fig 6.

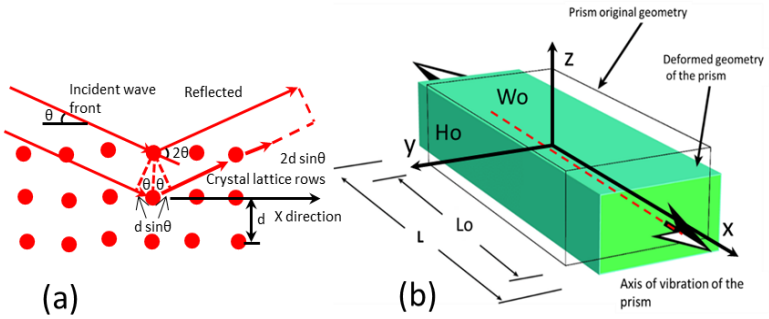

Fig 6. (a) Brillouin model of the crystalline medium; (b) Prismatic NaCl crystal geometry and eigen vibration mode.

Figure 6 is a reproduction of a figure of [10]. A prismatic sodium nanocrystal, with length L_o, height H_o, and width W_o, is aligned along the x-axis of the coordinate system. The crystal is excited by an evanescent electromagnetic field generated by a pumping laser light beam. According to the Brillouin model, the crystalline structure consists of rows and columns of spherical particles, separated by a distance "d" between the center of the spheres. The angle of incidence θ is the angle that produces the Bragg reflection and is the angle that we have called θ_{icrit}.

The vibrations of the crystal create two significant effects. First, this interaction can be understood through the inelastic impact of phonons, which transfer mechanical energy from phonons to photons.

The second effect involves changes in the density of the crystal. This creates a standing 3D grating that diffracts the scattered wavefronts and alters their trajectories. Figure 7(a) shows one of the images captured by the microscope using a ball lens. The procedure for obtaining the contours illustrated in Fig 7(a) is detailed in [8]. The formation process of Fig 7(b) is described in [10].

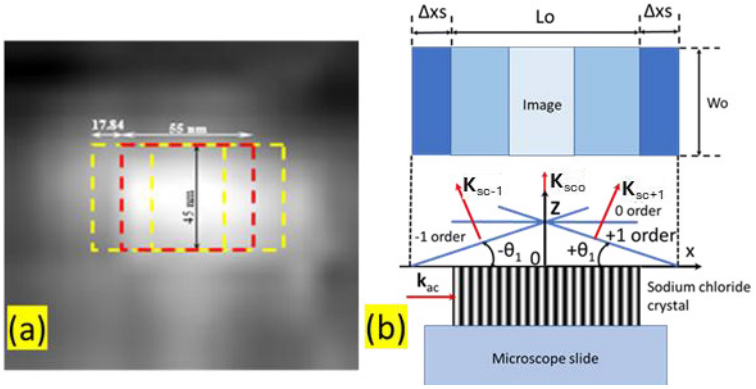

Fig 7. (a) NaCl single nanocrystal of dimensions 55×45 nm level of gray image; (b) Process of formation of the observed image.

Next, it is important to consider the momentum conservation conditions of the scattered field. The crystal vibrates axially, and as shown in Fig 7(b), three main orders are emitted by the crystal: the zero order and the ±1 orders. As illustrated in Fig 7(b), the zero-order of the scattered wavefront aligns with the normal to the face of the prism, which is also the viewing direction of the microscope. The wave vector of the zero-order illumination beam, $\mathbf{K}_{sco}$ (that may be denoted also as $\mathbf{K}_{sct,0}$), is perpendicular to the acoustic wave vector, $\mathbf{K}_{ac}$. The ±1 orders, at angles ± θ, produce the shifted images observed at the image plane, represented by the corresponding wave vectors $\mathbf{K}_{sc+1}$ and $\mathbf{K}_{sc-1}$ (that may be denoted also as $\mathbf{K}_{sct+1}$ and $\mathbf{K}_{sct-1}$, respectively).

Figure (8) shows the gray levels of the image of the crystal of Fig 7(a). Due to the structure of the standing wave, most of the energy is concentrated in the aforementioned zero and ±1 orders [9]. The vectorial representation of the conservation of momentum shown in Fig (4) can be related to Fig 8.

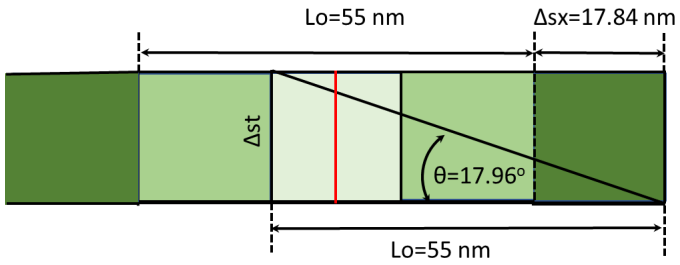

Fig 8. Graphical representation of the relationship between the shift Δ_{sx}, the length L_o and the angle θ.

The following relationship can be derived from Fig (8), $\Delta_{st} = \Delta_{sx} = L_o \times \tan(\theta)$, that is $\Delta_{st} = \Delta_{sx} = 55\text{nm} \times \tan(17.96°) = 17.84$ nm to four significant figures. In [9], it is proved that the values of Δ_{sx} can be calculated using an alternative procedure from that used in [8], defining a parameter "p_p". The statistical analysis of the data indicates that the values of Δ_{sx} obtained by both methods agree well within the limits of statistical dispersion. Figure 9 shows that the shift values Δ_{sx} correlate with the values of $2p_p$ at $R^2 = 0.9994$.

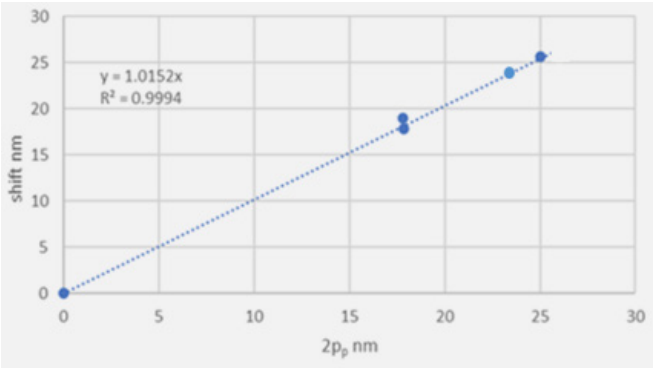

Fig 9. Correlation between the shift Δ_{xs} measured with the method applied in [8] and the parameter "p_p" obtained from the procedure explained in [10].

In conclusion, the shift Δ_{xs} for prismatic crystal whose face is parallel to the image plane of the recording camera is a linear function of the length L_o. It is noteworthy that the software used to determine the crystal's dimensions relies on the gray levels of the recorded images; all information from the color channels is ignored. The calibration procedures are also done in the grayscale.

5 Introducing color as a variable in the NF system

The correlation between the color of light emitted by excited crystals and the dimensions H_o and L_o of those crystals introduces a new variable: the wavelength (λ_{sct}) of the emitted light, which is dependent on the wavelength of the pumping laser. In Fig (10), the wavelengths of the wavefronts produced by four single sodium crystals analyzed in [8] are plotted against the length L_o of the crystal. The point on the wavelength axis corresponds to the wavelength of the illuminating laser, which is $\lambda = 632.8$ nm. Based on the correlation equation for λ vs L_o, the wavelength λ is 624.32 nm. The difference between this wavelength and that of the laser is 1.34%, indicating substantial agreement between the model and the experimental results. From Fig 6(a), the length of the crystal $L_o = N_{at} \times d$, where N_{at} is the number of atoms in a row.

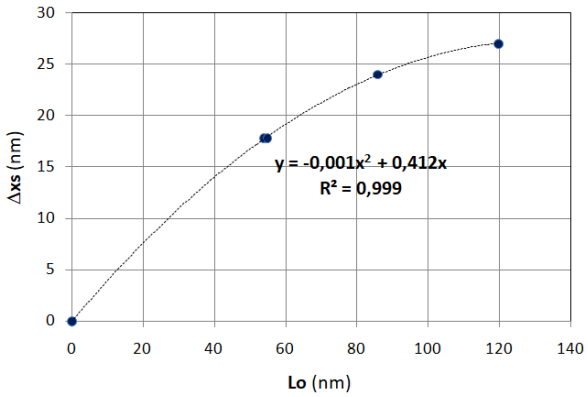

Fig 10. Variation of emerging wavelengths from the sodium crystals analyzed in [8] with respect to crystal's length L_o.

The conclusion is that crystal dimensions, specifically L_o, correlate with the color of light emission. This correlation is important for metrology and for determining the properties of the materials of the observed objects

6 The energy balance and momentum balance of the whole system

The simplification made on the conservation of momentum (see Fig 4) yield that that the vectorial triangle expressing the conservation of momentum is an isosceles triangle. In the case of NaCl crystals shown in Fig 7(b) the following momentum vectors are generated $\mathbf{K}_{sc}$ and $\mathbf{K}_{sc+1}$, $\mathbf{K}_{sc-1}$.

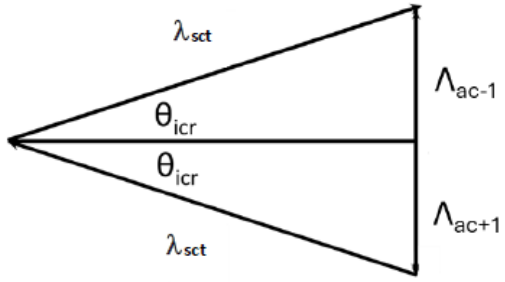

Fig 11. Graphical representation of the isosceles triangle expressing the conservation of momentum of the whole system of the image recorded when a ball lens produces the image.

Figure 11 graphically represents the vector equation that reflects the momentum conservation in the crystal depicted in Fig 7(b). To connect the graphical representation of the vectorial equation shown in Fig 11 with the image formation in Fig 8 and Fig 7(b), we need to refer back to Eq (10), which relates θ_{icri}, λ_{sct}, and Λ_{ac}. This connection is established through Eq (11) as,

$$\Delta_{xs} = L_o \times \tan\theta_{icri} \tag{11}$$

Equation (10) corresponds to the standing wave in the crystal, which creates the grating that diffracts the wavefronts emitted by the crystal. The next step is summarized in Table 2.

Table 2 presents the data for the crystals analyzed in [8]. The crystal with a characteristic length (L_o) of 86 nm has a step on its upper face, which means that the procedures used for the other crystals do not yield accurate results. Therefore, the correlation shown in Fig 10 was applied to determine the shift for L_o= 86 nm. This value aligns well with the subsequent results included in this analysis.

Table 2. Relationship between nano-crystal size and photon-phonon interaction parameters.

i) L_o (nm)	1) Δ_{xs} (nm)	2) tanθ_{icri}	3) θ_{icri}	4) sinθ_{icri}	5) λ_{sct} (nm)	6) n_r	7) λ_{cst} (nm)	8) Λ_{ac} (μm)
54	17.80	0.3296	18.24	0.312	557	1.555	358.19	1.6
55	17.84	0.3243	17.96	0.3083	556	1.555	357.55	1.59
86	24	0.279	15.589	0.2687	524	1.557	336.54	1.252
120	27	0.216	14.59	0.252	480	1.561	307.49	1.22

Column "i" gives crystal lengths L_o from [8]. Column "1" provides the values of the shifts Δ_{xs} from [8], except for the correction related to the crystal L_o= 86 nm. Column "2" gives the values of tanθ_{icri}, where θ_{icri} is the angle corresponding to the standing wave in the crystal given by Eq (10), and whose tangent can be computed by Eq (11), tanθ_{icri}= Δ_{xs}/L_o. Column "3" gives the values of the angles θ_{icri} in degrees. Column "4" gives the values of sinθ_{icri}. Column "5" presents the values of scattered light wavelengths in air (vacuum) λ_{sct}. The corresponding values of λ_{sct} were derived from the correlation shown in Fig 10. Column "6" was obtained from literature and shows the values of NaCl refraction index for different light wavelengths. Column "7" gives the value of the scattered wavelength inside crystal λ_{sct} that can be obtained from the information given in columns"5" and "6". Column "8" gives the acoustic wavelength Λ_{ac}, which can be obtained from the conservation of momentum graph of Fig 12.

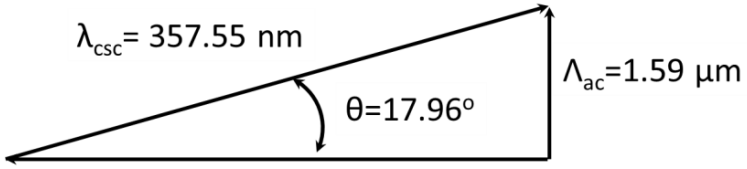

Fig 12. Vectorial representation of the conservation of momentum for the standing wave.

Figure (12) is derived from the arguments describing the pattern of Fig 8. From the mentioned analysis one gets the equation

$$\sin\theta_{icri} = \frac{\lambda_{sct}}{\Lambda_{ac}} \tag{12}$$

After applying usual trigonometric transformations to Eq (12), one obtains the values of Λ_{ac}.

Figure 11 represents the momentum balance for the light wavefronts travelling in the optical system of Fig 7(b), also including the wavefronts that are diffracted by the standing diffraction grating. In [9,10], it is shown that the grating concentrates most of the energy of the wavefronts in the mentioned diffraction orders. To find out that the values given in Column "8" align with values quoted in the literature, it is necessary to make additional derivations.

Table 3 shows the values of photon-phonon interaction parameters for the NaCl nano-crystals analyzed in [8] using the optical system of Fig 7(b). The table also shows the computed values of sinθicr and the corresponding values of this angle in degrees. With this information, the value of v_{ac} can be computed. Let us refer to the optical set up schematized in Fig 7(b) to visualize the mechanisms of energy conservation and momentum conservation for the propagating wavefronts. Although a stationary wave is present, two propagating waves move back and forth between the two ends of each analyzed NaCl nano-crystal. As is done previously, it can be introduced the approximation of the order of magnitude used to obtain Eq (7), $v_{sc} \approx v_L$. One obtains,

$$v_{ac} = 2\sin\theta_{icri} \times v_L \tag{13}$$

The reference [11] gives the value of v_{ac} = 4700 m/s. This value corresponds to the propagation of the wave given by Eq (9). Since we have a standing wave, Eq (10) applies and v_{ac} = 1/2×4700 m/s = 2350 m/s. This value fits well with the values of Table 3.

Table 3. Relationship between nano-crystal size and photon-phonon interaction parameters for the system of Fig 7(b).

Lo (nm)	λ_{sct} (nm)	Λ_{ac} (μm)	$\sin\theta_{icr}$	θ_{icr}	v_{ac} (m/s)	f_T (GHz)
54	557	1.6	0.348	20.36^o	2088	1.317
55	556	1.59	0.349	20.43^0	2094	1.320
86	524	1.25	0.419	24.77^o	2514	2.011
120	480	1.22	0.393	23.14^o	2358	2.080

The temporal frequency of the ultrasound waves can be computed from the equation,

$$f_T = \frac{v_{ac}}{\Lambda_{ac}} \tag{14}$$

The values f_T in Table 3 are of the correct order of magnitude for phonons. It is possible to introduce the argument that the fact that the values of v_{ac} are validated by [10] indicates that the values of Λ_{ac} of column "8" of Table 2 have a validation in the literature of phonons. *This concussion* indicates that one has a tool to obtain the information that provides the values of H_o and L_o in the nanometer range.

7 Discussion and conclusions

Incorporating the emitted light wavelength λ_{sct} as a variable in the Nano Fraction system offers a valuable tool for various technological and scientific applications. Due to the paper's length constraints, it was not feasible to include all applications of the 2D subset of Nano Fraction, particularly in analyzing defects in semiconductors that have been validated using atomic force microscopy. Additionally, biomedical applications of this methodology encompass the study of viruses and other organic material-related issues.

References

1. Sciammarella C A, Lamberti L, Sciammarella E, Sciammarella F M, Santoro L, Digital Holographic Moiré Generalized Nano-Fraction, *Exp Mech*, (2025), Special Issue Celebrating the 100th Anniversary of Prof Cesar A Sciammarella (To appear).
2. Brillouin L, Wave Propagation in Periodic Structures, (McGraw-Hill Book Company, New York, USA), 1946.
3. Brillouin L, Les Tenseurs en Mécanique et en Elasticité, Chapter 3. Vibration des solides et les quanta, pp 312-319. Masson & C, Paris, France, (1949).
4. Garmire E, Stimulated Brillouin review: Invented 50 years ago and applied today, *Int J Opt*, 2018(2018)2459501; doi. org/10.1155/2018/2459501.
5. Polo J A, Mackay T G, Lakhtakia A, Electromagnetic Surface Waves: A Modern Perspective, 1st Edn, (Elsevier, Amsterdam, The Netherlands), 2013.
6. Rucker R A, Summary on the Research of the Shroud of Turin, November 14, 2018.
7. Chiao R, Brillouin Scattering and Coherent Phonon Generation, Ph D Dissertation, Massachusetts Institute of Technology, 1965.
8. Sciammarella C A, Lamberti L, Sciammarella F, The equivalent of Fourier Holography at the nanoscale, *Exp Mech*, 49(2009)747–773.
9. Sciammarella F M, Sciammarella C A, Lamberti L, Nano-holographic interferometry for in vivo observations. In: Shaked N T, Zalevskey Z, Satterwhite L L (eds), Biomedical Optical Phase Microscopy and Nanoscopy, (Elsevier, The Netherlands), 2013, pp 353-385.
10. Sciammarella C A, Lamberti L, Sciammarella F M, Holography at the nano level with visible light wavelengths. In: Mihaylova E, (ed), Holography - Basic Principles and Contemporary Applications, (Intech, Rijeka, Croatia), 2013, pp 243–281.
11. Hsieh W-P, High-pressure thermal conductivity and compressional velocity of NaCl in B1 and B2 phase, *Sci Rep*, 11(2021)21321; doi. org/10.1038/s41598-021-00736-2.

[*Received*; 01.12.2024; *revised recd*: 28.12.2024; *accepted*: 30.12.2024]